

## Inelastic nuclear screening for different secondaries produced in $p + \text{Pb}$ collisions at LHC energy

G. H. Arakelyan,<sup>1,\*</sup> C. Merino,<sup>2,†</sup> Yu. M. Shabelski,<sup>3,‡</sup> and A. Shuvaev<sup>3,§</sup>

<sup>1</sup>*A. Alikhanyan National Scientific Laboratory (Yerevan Physics Institute), Yerevan 0036, Armenia*

<sup>2</sup>*Departamento de Física de Partículas, Facultade de Física and Instituto Galego de Física de Altas Enerxías (IGFAE) Universidade de Santiago de Compostela, Galiza 15782, Spain*

<sup>3</sup>*Petersburg Nuclear Physics Institute NCR Kurchatov Institute Gatchina, St.Petersburg 188300 Russia*

(Received 20 June 2016; revised manuscript received 6 September 2016; published 11 April 2017)

We calculate the inclusive spectra of secondaries produced in soft (minimum-bias)  $p\text{Pb}$  collisions in the framework of the quark-gluon string model at LHC energy, by taking into account the inelastic screening corrections (percolation effects). The role of these effects is expected to be very large at the very high energies, and they should decrease the spectra more than 2 times in the midrapidity region at  $\sqrt{s_{NN}} = 5 \text{ TeV}$ .

DOI: [10.1103/PhysRevD.95.074013](https://doi.org/10.1103/PhysRevD.95.074013)

### I. INTRODUCTION

The investigation of soft interactions in high energy  $p + \text{Pb}$  collisions is very interesting because it provides information about inelastic shadow corrections [1,2] for inclusive particle production.

In [1,2] it was shown that in the frame of the quark-gluon string model (QGSM) one can obtain a reasonable description of the experimental data on the inclusive spectra of secondaries produced in  $d + \text{Au}$  collisions at  $\sqrt{s} = 200 \text{ GeV}$  (RHIC), by accounting of the inelastic corrections, which are related to the multipomeron interactions. These corrections lead to the saturation of the inclusive density of secondary hadrons in the soft (low  $p_T$ ) region, where the methods based on perturbative QCD cannot be used. The effects of the inelastic shadow corrections should increase with the initial energy. The difference in the results for the spectra obtained from the calculations with and without the inelastic shadow effects at LHC energies is of about a factor 2 in the midrapidity region.

The applicability of our approach seems also to be supported by the comparison of our calculations [3] with the data of the ALICE collaboration [4] at  $\sqrt{s_{NN}} = 5 \text{ TeV}$ .

In principal, two possibilities exist to explain the origin of the inelastic nuclear screening: either it comes from the diagrams with Pomeron interactions, or from the interactions of the produced secondaries with another hadrons. In the first case, the inelastic screening effects should be the same for different secondaries, while for the second one these effects should depend on the interaction cross sections of the secondaries, so the effects should be different for the different secondaries.

In this paper we compare the experimental data for the inclusive densities of different secondaries obtained by the CMS [5] collaboration to the corresponding results obtained in the frame of the QGSM [6,7] for  $p + \text{Pb}$  at  $\sqrt{s_{NN}} = 5 \text{ TeV}$ .

The QGSM quantitatively describes many features of the high energy production processes, including the inclusive spectra of different secondary hadrons produced in the high energy hadron-nucleon [8–12] and hadron-nucleus collisions [13,14]. In the frame of the QGSM, the hadron-nucleon interactions have already been considered at different energies, including LHC. The hadron-nucleus collisions have been described at energies up to the LHC range by using the standard Glauber-Gribov multiple scattering theory, based on the dominance of eikonal diagrams, thus indicating that the inelastic screening effects are negligibly small [1] for energies under the very high values available at LHC. Now, at the LHC energies the inelastic screening corrections for secondaries production in hadron-nucleus collisions become large, which allows us to analyze them in more detail.

The effect of the inelastic screening corrections on the inclusive spectra for nuclear targets can be also crucial in the frame of other alternative candidates for the theoretical description of particle production at high and very high energies, that we do not consider in this paper, such as color glass condensate model, statistical model of particle production, and the models based on the standard nuclear PDF's.

### II. INCLUSIVE SPECTRA OF SECONDARY HADRONS IN THE QUARK-GLUON STRING MODEL

In order to produce quantitative results for the inclusive spectra of secondary hadrons, a model for multiparticle production is needed. It is for that purpose that we have

\* argev@mail.yerphi.am

† merino@fpaxp1.usc.es

‡ shabelsk@thd.pmpi.spb.ru

§ shuvaev@thd.pmpi.spb.ru

used the QGSM [6,7] in the numerical calculations presented below. The QGSM is based on the Reggeon calculus and on the  $1/N_c$  (or  $1/N_f$ ) expansion in QCD, where  $N_c$  and  $N_f$  are the numbers of colors and light flavors, respectively. It is worthwhile to note here that the real expansion parameters are  $1/N_c^2$  (or  $1/N_f^2$ ), which allows us to consider them as being rather small.

Both the high energy hadron-nucleon and hadron-nucleus interactions are treated in the QGSM as proceeding via the exchange of one or several Pomerons. The elastic and inelastic processes result from cutting through or between Pomerons [15]. Each Pomeron corresponds to a quark-gluon cylinder diagram. The cut through the cylinder produces two showers of secondaries (color strings) [16,17]. The decay of these strings generates new quark-antiquark pairs that lead then to the production of secondary hadrons. This picture of particle production is very close to that of the Lund model [17].

The cylinder diagram which correspond to Pomeron exchange is shown in Fig. 1(a), in which the cylinder boundaries are drawn by the dash-dotted vertical lines, its surface is schematically depicted by dashed curves, and the solid curves at the top and bottom stand for the beam and target quarks whose interaction is mediated by this cylinder exchange. The newly produced quark-antiquark pairs shown in Fig 1(b) by solid curves. The inclusive spectrum of secondaries is then determined by the convolution of diquark, valence quark, and sea quark distributions in the incident particles,  $u(x, n)$ , with the fragmentation functions of quarks and diquarks into the secondary hadrons,  $G(z)$ . Both functions  $u(x, n)$  and  $G(z)$  are determined by the appropriate Reggeon diagrams [18]. Note that the quark-antiquark distributions  $u(x, n)$  differ from the standard PDF's extracted from fits to experimental data because the  $u(x, n)$  are theoretically taken to be valid at the rather low  $Q^2$  which are relevant for soft processes, while the PDF distributions are obtained by fitting the experimental behavior at large  $Q^2$ . The diquark and quark distribution functions depend on the number  $n$  of cut Pomerons in the considered diagram. In the following calculations we use the recipe of Ref. [13].

For the nucleon target, the inclusive density  $dn/dy$  of a secondary hadron  $h$  has the form [6]:

$$\frac{dn}{dy} = \frac{1}{\sigma_{\text{inel}}} \cdot \frac{d\sigma}{dy} = \frac{x_E}{\sigma_{\text{inel}}} \cdot \frac{d\sigma}{dx_F} = \sum_{n=1}^{\infty} w_n \cdot \phi_n^h(x), \quad (1)$$

where the functions  $\phi_n^h(x)$  determine the contribution of diagrams with  $n$  cut Pomerons, and  $w_n$  is the probability for this process to occur [19]. Here we neglect the diffractive dissociation contributions that would only be significant in the fragmentation regions, i.e., at large  $x_F$ .

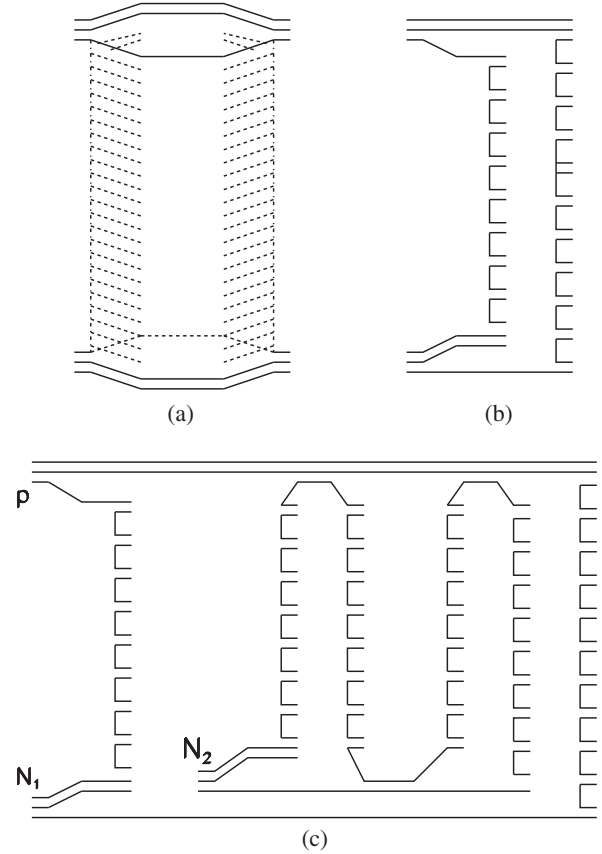


FIG. 1. (a) Cylindrical diagram representing the Pomeron exchange within the dual topological unitarization (DTU) classification (quarks are shown by solid lines); (b) Cut of the cylindrical diagram corresponding to the single-Pomeron exchange contribution in inelastic  $pp$  scattering; (c) Diagram corresponding to the inelastic interaction of an incident proton with two target nucleons  $N_1$  and  $N_2$  in a  $pA$  collision.

For  $pp$  collisions

$$\begin{aligned} \phi_n^h(x) = & f_{qq}^h(x_+, n) \cdot f_q^h(x_-, n) + f_q^h(x_+, n) \cdot f_{qq}^h(x_-, n) \\ & + 2(n-1)f_s^h(x_+, n) \cdot f_s^h(x_-, n), \end{aligned} \quad (2)$$

$$x_{\pm} = \frac{1}{2} \left[ \sqrt{4m_T^2/s + x^2} \pm x \right], \quad (3)$$

where  $f_{qq}$ ,  $f_q$ , and  $f_s$  are the contributions of diquarks, valence quarks, and sea quarks, respectively.

These contributions are determined by the convolution of the diquark and quark distributions with the fragmentation functions, e.g.,

$$f_q^h(x_+, n) = \int_{x_+}^1 u_q(x_1, n) \cdot G_q^h(x_+/x_1) dx_1. \quad (4)$$

The diquark and quark distributions, as well as the fragmentation functions, are determined by Regge

asymptotics [18]. The numerical values of the model parameters were published in Ref. [9].

The probabilities  $w_n$  in Eq. (1) are the ratios of the cross sections corresponding to  $n$  cut Pomerons,  $\sigma^{(n)}$ , to the total nondiffractive inelastic  $pp$  cross section,  $\sigma_{nd}$  [19].

The contribution of multipomeron exchanges in high energy  $pp$  interactions results in a broad distribution of  $w_n$  (see [3]). In the case of interaction with a nuclear target, the multiple scattering theory (Gribov-Glauber theory) is used, which allows us to treat the interaction with the nuclear target as the superposition of interactions with different numbers of target nucleons. Let  $W_{pA}(\nu)$  be the probability for the inelastic interactions of the proton with  $\nu$  nucleons of the target, and  $\sigma_{\text{prod}}^{pA}$  the total cross section of secondary production in a  $p + A$  collision. From the multiple scattering theory, one has:

$$W_{pA}(\nu) = \sigma^{(\nu)} / \sigma_{\text{prod}}^{pA}, \quad (5)$$

(see again Ref. [3] for the numerical examples). Here,

$$\sigma^{(\nu)} = \frac{1}{\nu!} \int d^2b \cdot [\sigma_{\text{inel}}^{pN} \cdot T(b)]^\nu \cdot e^{-\sigma_{\text{inel}}^{pN} \cdot T(b)} \quad (6)$$

coincides [20–23] with the optical model expression [24], and

$$\sigma_{\text{prod}}^{pA} = \int d^2b \cdot (1 - e^{-\sigma_{\text{inel}}^{pN} \cdot T(b)}), \quad (7)$$

where  $T(b)$  is the profile function of the nuclear target:

$$T(b) = A \int_{-\infty}^{\infty} dz \cdot \rho(b, z), \quad (8)$$

with  $\rho(r = \sqrt{b^2 + z^2})$  the one-particle nuclear density.

The average value of  $\nu$  has the well-known form:

$$\langle \nu \rangle = \frac{A \cdot \sigma_{\text{inel}}^{pp}}{\sigma_{\text{prod}}^{pA}}. \quad (9)$$

We use the numerical values  $\sigma_{\text{inel}}^{pp} \approx 72$  mb and  $\sigma_{\text{prod}}^{pPb} \approx 1900$  mb at  $\sqrt{s} = 5$  TeV, so that

$$\langle \nu \rangle_{p+Pb} \approx 7.9. \quad (10)$$

In the calculation of the inclusive spectra of secondaries produced in  $pA$  collisions we should consider the possibility of one or several Pomeron cuts in each of the  $\nu$  blobs of the proton-nucleon inelastic interactions. For example, in Fig. 1(c) it is shown one of the diagrams contributing to the inelastic interaction of a beam proton with two nucleons from the target. In the blob of the proton-nucleon(1) interaction one Pomeron is cut, and in the blob

of the proton-nucleon(2) interaction two Pomerons are cut. It is essential to take into account all the diagrams with every possible Pomeron configuration and its permutations. The diquark and quark distributions and the fragmentation functions here are the same as in the case of the interaction with one nucleon.

The process shown in Fig. 1(c) satisfies [20–23] the condition that the absorptive parts of the hadron-nucleus amplitude are determined by the combination of the absorptive parts of the hadron-nucleon amplitudes.

### III. INCLUSIVE SPECTRA IN $p + A$ COLLISIONS AT VERY HIGH ENERGY AND INELASTIC SCREENING (PERCOLATION) EFFECTS

The QGSM gives a reasonable description [13,25] of the inclusive spectra of different secondaries produced in hadron-nucleus collisions at energies  $\sqrt{s_{NN}} = 14\text{--}30$  GeV.

The situation drastically changes at RHIC energies, where, from a theoretical point of view, the authors of Ref. [1] (see this reference for a detailed discussion on this point) claimed, after comparing in the central (midrapidity) region the theoretical inclusive densities with and without (superposition picture [26–28]) saturation effects, for  $Pb\text{-}Pb$  collisions at RHIC energies, that the suppression factor in the inclusive density for  $Pb\text{-}Pb$  collisions when taken into account saturation effects was of about 2. Later, his effect was experimentally confirmed, since while the spectra of secondaries produced in  $pp$  collisions could be rather well described, when comparing the theoretical inclusive densities without saturation effects to the corresponding RHIC experimental data for  $Au\text{-}Au$  collisions [29,30], clear evidence for the inclusive density saturation effects which reduce the inclusive density appeared, though the suppression factor obtained in this case was of 1.6. To be theoretically consistent, and since we are not considering the case of  $Au\text{-}Au$  collisions in this paper, we have used the suppression factor equal to 2 in our calculations.

This reduction can be explained by the inelastic screening corrections connected to multipomeron interactions [1]. The effect is very small for integrated cross sections (many of them are determined only by geometry), but it is very important [1] for the calculations of secondary multiplicities and inclusive densities at the high energies.

However, all estimations are model dependent. The numerical weight of the contribution of the multipomeron diagrams is rather unclear due to the many unknown vertices. The number of unknown parameters can be reduced in some models, and, for example, in Ref. [1] the Schwimmer model [31] was used for the numerical estimations.

Other approaches were used in Ref. [32], where the phenomenological multipomeron vertices of eikonal type were introduced for enhancement diagram summation.

The calculations of inclusive densities and multiplicities, both in  $pp$  [33,34], and in heavy ion collisions [34,35] (with accounting for inelastic nuclear screening), can be

fulfilled in the percolation theory, and they result in a good agreement with the experimental data in a wide energy region.

The percolation model also provides a reasonable description of the transverse momentum distribution (at low and intermediate  $p_T$ ) including the Cronin effect and the behavior of the baryon/meson ratio [36–38]. The percolation approach assumes two or several Pomerons to overlap in the transverse space and to fuse in a single Pomeron. Given a certain transverse radius, when the number of Pomerons in the interaction region increases, at least part of them may appear inside another Pomeron. As a result, the internal partons (quarks and gluons) can split, leading to the saturation of the final inclusive density. This effect persists with the energy growth until all the Pomerons will overlap [36,37,39].

In order to account for the percolation effects in the QGSM, it is technically more simple [2] to consider in the central region the maximal number of Pomerons  $n_{\max}$  emitted by one nucleon. After they are cut, these Pomerons lead to the different final states. Then the contributions of all the diagrams with  $n \leq n_{\max}$  are accounted for as at the lower energies. The unitarity constraint also obeys the emission of the larger number of Pomerons  $n > n_{\max}$  but due to fusion in the final state (on the quark-gluon string stage) the cut of  $n > n_{\max}$  Pomerons results in the same final state as the cut of  $n_{\max}$  Pomerons.

By doing this, all model calculations become rather simple and very similar to those in the percolation approach. The QGSM fragmentation formalism allows one to calculate the spectra of different secondaries integrated over  $p_T$  as functions of initial energies, rapidity, and  $x_F$ . In this scenario we obtain a reasonable agreement with the experimental data on the inclusive spectra of secondaries at RHIC energy (see [2] with  $n_{\max} = 13$ ).

It has been shown in [40] that the number of strings for the secondary production should increase with the initial energy even when the percolation effects are included. Thus, in the following calculations we use the value  $n_{\max} = 21$  at the LHC energy  $\sqrt{s} = 5$  TeV, that can be regarded as the normalization of all the charged secondaries multiplicities in the midrapidity region to the ALICE data [4]. The predictive power of our calculation applies for different sorts of secondaries in midrapidity region. If the inelastic nuclear screening comes mainly from the Pomeron interactions, as it was discussed above, the screening effects would be the same for all the secondaries. On the other hand, if the final state absorption of the produced particles are important, nuclear screening effects would be different for different secondaries, i.e. for kaons and antibaryons.

In the following calculations, one additional effect is also taken into account, namely the transfer of the baryon charge to large distances in rapidity space through the string junction effect [10,11]. This transfer leads to an asymmetry in the production of baryons and antibaryons in the central

region that is nonzero even at LHC energies. In the calculation of these effects, the following values have been chosen for the model parameters [11]:

$$\alpha_{SJ} = 0.5 \quad \text{and} \quad \varepsilon = 0.0757. \quad (11)$$

#### IV. RAPIDITY SPECTRA OF DIFFERENT SECONDARIES AT LHC ENERGIES

To compare the calculated effect of nuclear screening with the experimental data, the adequate description of the secondary production on nucleon, as well as on nuclear targets is needed. First, we present the QGSM description of  $\pi^\pm$ ,  $K^\pm$ ,  $p$ , and  $\bar{p}$  productions in  $pp$  collisions at LHC energies, and then we compare the results of our calculations with the experimental data by the CMS Collaboration [5,41] and by the ALICE Collaboration [42–44], as it is shown in Fig. 2, where, following the analysis published by the ALICE Collaboration [44], the productions of average  $\pi$ ,  $K$ , and  $p\bar{p}$  are presented.

As it can be seen in Fig. 2, the experimental data by the ALICE Collaboration are approximately 20%–30% lower than those published by the CMS Collaboration. Probably, the samples published by the two collaborations were obtained in slightly different experimental conditions, and our QGSM results cannot determine which sample is better suited to compare with.

In spite of this disagreement between ALICE and CMS data shown in Fig. 2, our QGSM result is qualitatively

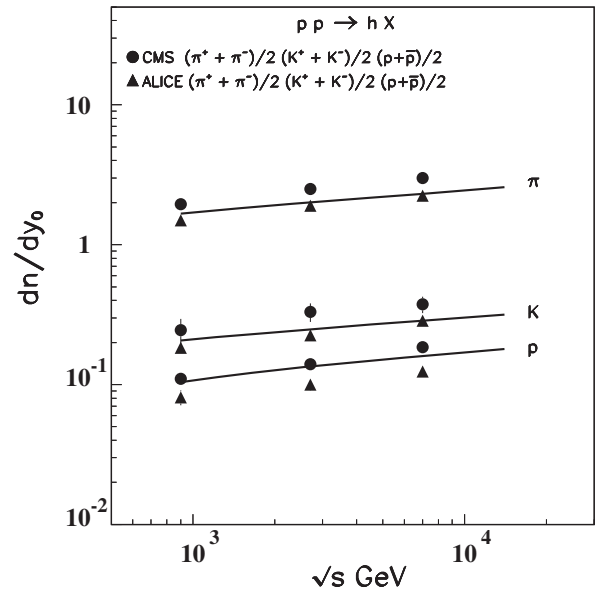


FIG. 2. The energy dependence of the rapidity density  $dn/dy$  at  $y = 0$  of average pions, kaons, and protons/antiprotons production in  $pp$  collisions. The experimental data are by the CMS Collaboration [5,41] and by the ALICE collaboration [42–44]. The theoretical curves represent the result of the corresponding QGSM calculations.

compatible with both experimental samples. The calculation of the values of Pomeron parameters in QGSM is well established by Regge theory, and the uncertainty generated by the calculation of these values is negligible when compared to other sources of uncertainties in the model, as it was well established in Ref. [45]. Actually, the main source of intrinsic uncertainties in the results obtained by using QGSM is related to some indeterminations in the specific polynomial form of the fragmentation functions [6,18] in the region of intermediate  $x_F$ , and in the values of some (few) free parameters appearing in the parametrization of this polynomial form. The theoretical uncertainty originated in QGSM by this effect is estimated to be on the level of 10%–15% [6], which has been largely supported along the years by the systematic comparison of our previous published results to experimental data. In this case, and due to this theoretical uncertainty, our QGSM results cannot univocally discriminate which one, if any, of these two sets of experimental data is actually correct.

The experimental point by the ALICE Collaboration [4],  $dn_{ch}/d\eta = 16.81 \pm 0.71$  at  $\sqrt{s_{NN}} = 5$  TeV has been used [3] to normalize the QGSM calculations for the case of nuclear targets. The agreement of our calculations with this result is reached at  $n_{\max} = 21$ , where the theoretical value is of  $dn_{ch}/d\eta = 16.28$  (see Ref. [3]). Later, the experimental value  $dn/dy(|y| \leq 1) = 19.1 \pm 0.2$  has been published by the CMS Collaboration [5], while the QGSM calculation gives  $dn/dy(|y| \leq 1) = 19.11$  with  $n_{\max} = 21$ , so it seems reasonable to use this  $n_{\max}$  value in our analysis.

The experimental data for  $p + \text{Pb}$  collisions by the CMS Collaboration on the inclusive densities of different secondaries,  $\pi^\pm$ ,  $K^\pm$ ,  $p$ , and  $\bar{p}$  [5] are presented in Table I, where they are compared with the results of our QGSM calculations. The agreement for every secondary particles is good, what it means that the experimental nuclear shadowing factor is the same for different secondaries, as it is assumed in our calculations.

Also in Table I, we present the QGSM results for the  $pp$  collisions at the same energy. The ratios of particle yields in

TABLE I. Experimental data on  $dn/dy$ ,  $|y| \leq 1$  by the CMS Collaboration [5] of charged pions, kaons,  $p$ , and  $\bar{p}$  production in central  $p + \text{Pb}$  collisions at  $\sqrt{s_{NN}} = 5$  TeV, together with the corresponding QGSM results. The parameter  $r$  is the ratio of the particle yields in  $p + \text{Pb}$  and  $pp$  reactions. The results of the QGSM calculations for  $pp$  collisions are also given.

| particles | CMS Collaboration<br>$dn/dy$ , $ y  \leq 1$ [5] | QGSM          |       |      |
|-----------|---|---------------|-------|------|
|           |   | $p+\text{Pb}$ | $pp$  | $r$  |
| $\pi^+$   | $8.074 \pm 0.087$                               | 8.103         | 2.190 | 3.70 |
| $\pi^-$   | $7.971 \pm 0.079$                               | 7.923         | 2.147 | 3.69 |
| $K^+$     | $1.071 \pm 0.069$                               | 1.006         | 0.273 | 3.69 |
| $K^-$     | $0.984 \pm 0.047$                               | 0.996         | 0.271 | 3.66 |
| $p$       | $0.510 \pm 0.018$                               | 0.545         | 0.150 | 3.63 |
| $\bar{p}$ | $0.494 \pm 0.017$                               | 0.536         | 0.148 | 3.62 |

$p + \text{Pb}$  and  $pp$  collisions are equal to 3.6–3.7, i.e., they are two times smaller than the values of  $\nu_{p+\text{Pb}}$  in Eq. (10). In the absence of inelastic nuclear screening, the ratio  $r = p\text{Pb}/pp$  in the midrapidity region should be equal to  $\nu_{p+\text{Pb}}$  [20–23], that is, to the average number of the inelastic collisions of the incident proton in the target nucleus. Thus, we can see that the inelastic nuclear screening factor is little larger than 2, and it is practically the same for all considered secondaries.

Our results for hyperon and antihyperons production in  $pp$  and  $p + \text{Pb}$  collisions at the same energy  $\sqrt{s} = 5$  TeV are presented in Table II.

The ratios of the inclusive densities of all secondary hyperons and antihyperons produced on Pb and hydrogen targets are practically the same as for secondary mesons production, with a  $\sim 5\%$  accuracy (see Tables I and II). If our theoretical results will be experimentally confirmed, that would indicate that the main contribution to the processes of hyperon and meson production has a similar nature.

Other theoretical models and approaches have also been used to describe the experimental data we consider in this paper, and to provide the corresponding predictions for nucleon-nucleus collisions at the LHC energies. Sometimes, though, the results published by these models are not directly comparable with those we show here.

While QGSM is based on the Regge (Pomeron) approach for the high energy interactions, the approach of the other models is to try to extend the QCD interaction picture to the large distances (or small virtualities) regime. These models are based on the color glass condensate (CGC) formalism [46,47], a self-consistent effective QCD theory at high energy in which one resums quantum corrections which are enhanced by large logarithms of  $1/x$  and that also incorporates nonlinear gluon saturation effects. In CGC the hadron production in proton-nucleus collisions also takes place in two stages: first, the production of gluons (theoretically under control), and the subsequent decay of gluon-jets into hadrons (fragmentation that has to be treated phenomenologically). Examples of this CGC-based model are the impact parameter dependent dipole saturation model (IP-Sat) [48] and the running

TABLE II. The QGSM results for the densities of hyperons and antihyperons production  $dn/dy_{y=0}$ , in  $p + \text{Pb}$  and  $pp$  collisions at  $\sqrt{s} = 5.02$  TeV.

| particles        | $p + \text{Pb}$ $dn/dy_{y=0}$ | $pp$ $dn/dy_{y=0}$ | $r$  |
|------------------|-------------------------------|--------------------|------|
| $\Lambda$        | 0.307                         | 0.0843             | 3.64 |
| $\bar{\Lambda}$  | 0.303                         | 0.0827             | 3.66 |
| $\Xi^-$          | 0.0250                        | 0.00676            | 3.70 |
| $\bar{\Xi}^+$    | 0.0248                        | 0.00669            | 3.70 |
| $\Omega^-$       | 0.00143                       | 0.000401           | 3.57 |
| $\bar{\Omega}^+$ | 0.00142                       | 0.000397           | 3.58 |

coupling Balitsky-Kovchegov model (rcBK) [49], which deal with gluon distributions in the dipole approach [50].

In particular, in Ref. [51] these two saturation models are applied to compute the minimum-bias average multiplicity at midrapidity for  $pA$  collisions, constrained by  $ep$  HERA data on inclusive and diffractive cross sections. The two models agree with the RHIC experimental data normalized to the PHOBOS 200 GeV dAu data [52], both the energy dependence of the average multiplicity, and the pseudorapidity,  $\eta$ , distributions, with an accuracy of  $\sim 10\%$ , that the authors explain is within the theoretical systematic uncertainty of the models. Also the corresponding predictions for LHC energies are presented.

A third saturation model is the color glass condensate b-CGC model [53,54], that explicitly includes the impact-parameter  $b$  dependence of the scattering amplitude, and other properties of the exact solution of the Balitskii-Kovchegov (BK) equation [55,56], and it also describes the small- $x$  HERA data. This model is employed in Ref. [57] to calculate the pseudorapidity distributions in pp and AA collisions at RHIC and LHC energies, as well as the corresponding predictions for pA collisions. While the b-CGC model does well for the pseudorapidity distributions, it does less well relative to the IP-Sat model for the pseudorapidity distribution [51].

In Ref. [58], the results by the Kharzeev-Levin-Nardi (KLN) model [59], for the pseudorapidity distributions in pp, dA, and AA collisions at RHIC are presented, as well as the results for the LHC in pp and AA collisions, and predictions for pA collisions at the LHC. This model combines the Glauber approach to proton-nucleus and nucleus-nucleus collisions with an ansatz for the unintegrated parton distributions that accounts for the existence of a saturation momentum scale. The KLN model provides a good description of the pseudorapidity distributions both at RHIC and LHC energies, in particular of the centrality dependence of the charged particle multiplicity.

In Ref. [60], a collinear factorized perturbative QCD model is used by computing the nuclear modification factor,  $R_{pPb}(y=0, p_T < 20 \text{ GeV}/c) = dn_{pPb}/(N_{coll}(b)dn_{pp})$ , with an electron-nucleus global fit with different nuclear shadow distributions. Its predictions for pPb collisions at 4.4 A TeV were estimated to test the nuclear shadowing of parton distributions at LHC, and compared to the fixed  $Q^2$  shadow ansatz of the Monte Carlo Heavy Ion Jet Interacting Generator (HIJING) [61] models. In Fig. 1 of Ref. [60], HIJING predictions of charged particles pseudorapidity distribution  $dN_{ch}/d\eta$  for minimum-bias pPb collisions at 4.4 A TeV, both with and without shadowing corrections, as well as the ratio  $R_{pPb}(\eta)$  (for  $N_{coll}(MB) = 6.4$ ) are presented. They show that at forward pseudorapidity the suppression is higher for central than for minimum-bias pPb collisions.

The HIJING model is also applied in Ref. [62], now with updated parton distributions and a new set of parameters in

the two-minijet model that controls the total pp cross section and the central pseudorapidity density. The hadron spectra and multiplicity distributions are calculated and compared to experimental LHC pp data. Also predictions for pp, pPb, and PbPb at LHC energies are given. In Fig. 11 of [62], the pseudorapidity distributions of charged hadrons, both in dAu collisions at RHIC energy  $\sqrt{s} = 200 \text{ GeV}/n$ , and in dPb collisions at the LHC energies, are shown. For the dAu case, the two used HIJING models describe reasonably well the RHIC experimental data [63] by the STAR Collaboration within the experimental errors for different centralities and minimum-bias events. Both in dAu at RHIC and in dPb at LHC, the change of the pseudorapidity distribution due to the variation of the gluon nuclear shadowing parameter is much smaller in the d-nucleus case, than in the corresponding nucleus-nucleus case.

In Ref. [64], the EPOS phenomenological approach is considered. EPOS is based on the parton model, but it also incorporates elastic and inelastic parton ladder splitting. This inelastic splitting (bifurcation of parton ladders) leads to a modified hadronization process, a kind of collective hadronization of multiple, parallel parton ladders, on the target side, in the case of d-nucleus collisions. The authors claim this is the equivalent of string fusion, but contrary to the usual string fusion picture, here one does not have complete ladders behaving collectively, but only the bifurcated ones on the target side. The study of the rapidity dependence of the experimental results on the transverse momentum results in dAu collisions by the four RHIC experiments is presented. In Fig. 15 of this reference [64], the EPOS simulations for the pseudorapidity spectra of charged particles in minimum-bias dAu collisions are shown, and compared to the PHOBOS [65], STAR [66], and BRAHMS [67] collaborations. In Figs. 16 and 17, the pseudorapidity spectra for, respectively, central and peripheral dAu collisions, are also shown. The EPOS simulations get a good level of agreement when compared to the RHIC experimental data, allowing the authors to use these pseudorapidity spectra to normalize the  $p_T$  spectra, in which the authors are mainly interested.

Other models, called hybrid, are focused on a description of the relativistic heavy ion collisions, by taking into account the effects on the flow from the whole partonic system in the overlap volume of the collision. One example of this is the coupling of the a multi-phase transport (AMPT) model [68–70] with a hydrodynamical model to provide a more direct link to QCD variables and properties.

The results published by the models above in the shape of  $\eta$  distributions are sensitive to  $p_T$  dependence, while QGSM provides integrated over  $p_T$  spectra.

## V. CONCLUSION

As explained in the first part of this paper, QGSM is based on rigorous theoretical background. Some intrinsic

level of uncertainty in QGSM comes from slight arbitrariness in the parametrization of the fragmentation functions and in the values of some free parameters. The systematic use of the model and the extended in time comparison of its results with the experimental data by different collaborations has shown that at high energies these uncertainties are not larger than 10%–15%. QGSM conceptually differs from the approach of QCD-based parton models, that are more adequate at small distances (high  $Q^2$ ), and of Monte-Carlo models which contain many parameters of unknown values.

It is seen that the inelastic nuclear screening corrections at LHC energies are really large. For all the ratios of inclusive densities of the secondaries produced in lead and hydrogen targets

$$R\left(\frac{p+Pb}{pp}\right) = \frac{dn}{dy}(p+Pb)|_{|y|\leq 1} / \frac{dn}{dy}(pp)|_{|y|\leq 1} = 3.6\text{--}3.7, \quad (12)$$

instead of the values  $R\left(\frac{p+Pb}{pp}\right) = \langle \nu \rangle_{p+Pb} \approx 7.5\text{--}8.0$  that one would expect in the absence of this effect [see Eq. (10)].

The QGSM approach for high energy inelastic pp, p-nucleus, and nucleus-nucleus collisions with multiparticle production provides a natural explanation of the

independence of the nuclear screening effects on the type of the produced particles in the central region of inclusive spectrum, as the nuclear screening effects are practically the same (within our theoretical accuracy) for  $\pi^\pm$ ,  $K^\pm$ ,  $p$ , and  $\bar{p}$  production. This is opposed to what happens in the case of elastic (e.g.,  $\pi + N$ ) interactions, where one would have to look at the  $p_T$  spectra, that is not the subject of this paper, the elastic process  $\pi + N \rightarrow \Delta \rightarrow \pi + N$  being in any case strongly suppressed at high energies, as taking place via a  $s$ -channel resonance. If confirmed experimentally for high energy inelastic pp, p-nucleus and nucleus-nucleus collisions with multiparticle production, this fact would indicate that the interaction of secondaries in the final state would be negligibly small.

## ACKNOWLEDGMENTS

We thank C. Pajares for his valuable comments. This work has been supported by Russian Science Foundation Grant No. 14-22-00281, by the State Committee of Science of the Republic of Armenia, Grant-15T-1C223, by Ministerio de Ciencia e Innovación of Spain under project FPA2014-58293-C2-1-P and FEDER, and the Spanish Consolider-Ingenio 2010 Programme CPAN (CSD2007-00042), and by Xunta de Galicia, Spain (2011/PC043).

- 
- [1] A. Capella, A. Kaidalov, and J. Tran Thanh Van, *Heavy Ion Phys.* **9**, 169 (1999).
- [2] C. Merino, C. Pajares, and Yu. M. Shabelski, *Eur. Phys. J. C* **59**, 691 (2009).
- [3] C. Merino, C. Pajares, and Y. M. Shabelski, *Eur. Phys. J. C* **73**, 2266 (2013).
- [4] B. Abelev *et al.* (ALICE Collaboration), *Phys. Rev. Lett.* **110**, 032301 (2013).
- [5] S. Chatrchyan *et al.* (CMS Collaboration), *Eur. Phys. J. C* **74**, 2847 (2014).
- [6] A. B. Kaidalov and K. A. Ter-Martirosyan, *Yad. Fiz.* **39**, 1545 (1984) [*Sov. J. Nucl. Phys.* **39**, 979 (1984)]; *Yad. Fiz.* **40**, 211 (1984) [*Sov. J. Nucl. Phys.* **40**, 135 (1984)].
- [7] A. B. Kaidalov, *Yad. Fiz.* **66**, 2014 (2003) [*Phys. At. Nucl.* **66**, 1994 (2003)].
- [8] A. B. Kaidalov and O. I. Piskunova, *Yad. Fiz.* **41**, 1278 (1985) [*Sov. J. Nucl. Phys.* **41**, 816 (1985)].
- [9] Yu. M. Shabelski, *Yad. Fiz.* **44**, 186 (1986) [*Sov. J. Nucl. Phys.* **44**, 117 (1986)].
- [10] G. H. Arakelyan, A. Capella, A. B. Kaidalov, and Yu. M. Shabelski, *Eur. Phys. J. C* **26**, 81 (2002).
- [11] C. Merino, M. M. Ryzhinskiy, and Yu. M. Shabelski, *Eur. Phys. J. B* **62**, 491 (2009).
- [12] G. H. Arakelyan, C. Merino, C. Pajares, and Yu. M. Shabelski, *Eur. Phys. J. C* **54**, 577 (2008).
- [13] A. B. Kaidalov and K. A. Ter-Martirosyan, and Yu. M. Shabelski, *Yad. Fiz.* **43**, 1282 (1986) [*Sov. J. Nucl. Phys.* **43**, 822 (1986)].
- [14] Yu. M. Shabelski, *Z. Phys. C* **38**, 569 (1988).
- [15] V. A. Abramovsky, V. N. Gribov, and O. V. Kancheli, *Yad. Fiz.* **18**, 595 (1973) [*Sov. J. Nucl. Phys.* **18**, 308 (1974)].
- [16] X. Artru and G. Mennesier, *Nucl. Phys.* **B70**, 93 (1974).
- [17] B. Andersson, G. Gustafson, and C. Peterson, *Phys. Lett.* **71B**, 337 (1977); *Z. Phys. C* **1**, 105 (1979).
- [18] A. B. Kaidalov, *Yad. Fiz.* **45**, 1452 (1987) [*Sov. J. Nucl. Phys.* **45**, 902 (1987)].
- [19] K. A. Ter-Martirosyan, *Phys. Lett.* **44B**, 377 (1973).
- [20] Yu. M. Shabelski, *Yad. Fiz.* **26**, 1084 (1977) [*Sov. J. Nucl. Phys.* **26**, 573 (1977)]; *Nucl. Phys.* **B132**, 491 (1978).
- [21] L. Bertocchi and D. Treleani, *J. Phys. G* **3**, 147 (1977).
- [22] J. Weis, *Acta Phys. Pol. B* **7**, 851 (1976).
- [23] T. Jaroszewicz, J. Kwieciński, L. Leśniak, and K. Zalewski, *Z. Phys. C* **1**, 181 (1979).
- [24] J. S. Trefil and F. von Hippel, *Phys. Rev. D* **7**, 2000 (1973).
- [25] Yu. M. Shabelski, *Yad. Fiz.* **45**, 223 (1987) [*Sov. J. Nucl. Phys.* **45**, 143 (1987)]; *Z. Phys. C* **38**, 569 (1988).
- [26] A. Capella, C. Merino, and J. Tran Thanh Van, *Phys. Lett. B* **265**, 415 (1991).
- [27] Yu. M. Shabelski, *Z. Phys. C* **57**, 409 (1993).

- [28] N. Armesto and C. Pajares, *Int. J. Mod. Phys. A* **15**, 2019 (2000).
- [29] B. B. Black *et al.* (PHOBOS Collaboration), *Phys. Rev. Lett.* **85**, 3100 (2000).
- [30] K. Adcox *et al.* (PHENIX Collaboration), *Phys. Rev. Lett.* **86**, 3500 (2001).
- [31] A. Schwimmer, *Nucl. Phys.* **B94**, 445 (1975).
- [32] S. Ostapchenko, *Phys. Rev. D* **77**, 034009 (2008).
- [33] I. Bautista, C. Pajares, and J. Dias de Deus, *Nucl. Phys.* **A882**, 44 (2012).
- [34] I. Bautista, J. Dias de Deus, G. Milhano, and C. Pajares, *Phys. Lett. B* **715**, 230 (2012).
- [35] I. Bautista, C. Pajares, G. Milhano, and J. Dias de Deus, *Phys. Rev. C* **86**, 034909 (2012).
- [36] J. Dias de Deus, E. G. Ferreira, C. Pajares, and R. Ugoccioni, *Eur. Phys. J. C* **40**, 229 (2005).
- [37] C. Pajares, *Eur. Phys. J. C* **43**, 9 (2005).
- [38] L. Cunqueiro, J. Dias de Deus, E. G. Ferreira, and C. Pajares, *Eur. Phys. J. C* **53**, 585 (2008).
- [39] M. A. Braun, E. G. Ferreira, F. del Moral, and C. Pajares, *Eur. Phys. J. C* **25**, 249 (2002).
- [40] J. Dias de Deus and C. Pajares, *Phys. Lett. B* **695**, 211 (2011).
- [41] S. Chatrchyan *et al.* (CMS Collaboration), *Eur. Phys. J. C* **72**, 2164 (2012).
- [42] K. Aamodt *et al.* (ALICE Collaboration), *Eur. Phys. J. C* **71**, 1655 (2011).
- [43] B. Abelev *et al.* (ALICE Collaboration), *Phys. Lett. B* **736**, 196 (2014).
- [44] J. Adam *et al.* (ALICE Collaboration), *Eur. Phys. J. C* **75**, 226 (2015).
- [45] A. M. Lapidus, V. I. Lisin, K. A. Ter-Martirosyan, and P. E. Volkovitsky, *Yad. Fiz.* **24**, 1237 (1976) [*Sov. J. Nucl. Phys.* **24**, 648 (1976)].
- [46] F. Gelis, E. Iancu, J. Jalilian-Marian, and R. Venugopalan, *Annu. Rev. Nucl. Part. Sci.* **60**, 463 (2010).
- [47] J. Jalilian-Marian and Y. V. Kovchegov, *Prog. Part. Nucl. Phys.* **56**, 104 (2006).
- [48] H. Kowalski and D. Teaney, *Phys. Rev. D* **68**, 114005 (2003).
- [49] J. L. Albacete and Y. V. Kovchegov, *Phys. Rev. D* **75**, 125021 (2007).
- [50] P. Tribedy and R. Venugopalan, *Nucl. Phys.* **A850**, 136 (2011).
- [51] P. Tribedy and R. Venugopalan, *Phys. Lett. B* **710**, 125 (2012).
- [52] B. B. Back *et al.* (PHOBOS Collaboration), *Phys. Rev. Lett.* **93**, 082301 (2004).
- [53] G. Watt and H. Kowalski, *Phys. Rev. D* **78**, 014016 (2008).
- [54] E. Iancu, K. Itakura, and S. Munier, *Phys. Lett. B* **590**, 199 (2004).
- [55] I. Balitsky, *Nucl. Phys.* **463**, 99 (1996).
- [56] Yu. V. Kovchegov, *Phys. Rev. D* **61**, 074018 (2000).
- [57] A. H. Rezaeian, *Phys. Rev. D* **85**, 014028 (2012).
- [58] A. Dumitru, D. E. Kharzeev, E. Levin, and Y. Nara, *Phys. Rev. C* **85**, 044920 (2012).
- [59] D. E. Kharzeev, E. Levin, and M. Nardi, *Phys. Rev. C* **71**, 054903 (2005).
- [60] G. G. Barnaföldi, J. Barrette, M. Gyulassy, P. Levai, and V. Topor Pop, *Phys. Rev. C* **85**, 024903 (2012).
- [61] V. Topor Pop, M. Gyulassy, J. Barrette, and C. Gale, *Phys. Rev. C* **84**, 044909 (2011).
- [62] W.-T. Deng, X. N. Wang, and R. Xu, *Phys. Rev. C* **83**, 014915 (2011).
- [63] B. I. Abelev *et al.* (STAR Collaboration), [arXiv:nucl-ex/0703016](https://arxiv.org/abs/nucl-ex/0703016).
- [64] K. Werner, F.-M. Liu, and T. Pierog, *Phys. Rev. C* **74**, 044902 (2006).
- [65] B. B. Back *et al.* (PHOBOS Collaboration), *Phys. Rev. C* **70**, 061901 (2004).
- [66] J. Adams *et al.* (STAR Collaboration), *Phys. Rev. C* **70**, 064907 (2004).
- [67] I. Arsene *et al.* (BRAHMS Collaboration), *Phys. Rev. Lett.* **94**, 032301 (2005).
- [68] B. Zhang, C. M. Ko, B.-A. Li, and Z.-W. Lin, *Phys. Rev. C* **61**, 067901 (2000).
- [69] Z.-W. Lin and C. M. Ko, *Phys. Rev. C* **65**, 034904 (2002).
- [70] Z.-W. Lin, *Acta Phys. Pol. B Proc. Suppl.* **7**, 191 (2014).